VCSEL Thermal Sources: A Physics-Based Simulation Approach

VCSEL thermal sources: a physics-based simulation approach

1st Alberto Gullino
Consiglio Nazionale Ricerche (CNR) - IEIIT
Torino, Italy
alberto.gullino@cnr.it

2st Martino D'Alessandro
Politecnico di Torino - DET
Torino, Italy
martino.dalessandro@polito.it

3rd Valerio Torrelli
Politecnico di Torino - DET
Torino, Italy
valerio.torrelli@polito.it

4th Alberto Tibaldi
Politecnico di Torino - DET
Torino, Italy
alberto.tibaldi@polito.it

5th Francesco Bertazzi
Politecnico di Torino - DET
Torino, Italy
francesco.bertazzi@polito.it

6th Pierluigi Debernardi
Consiglio Nazionale Ricerche (CNR) - IEIIT
Torino, Italy
pierluigi.debernardi@cnr.it

***Abstract*—Fully-comprehensive physics-based simulations of vertical-cavity surface-emitting lasers (VCSELs) must account for the coupled electrical, optical and thermal problems. While electrical and optical solvers form the foundation of cold-cavity VCSELs modeling, self-heating has the strongest impact during the device operation. In this work, we present the capability of our in-house solver VENUS to model the wavelength red-shift induced by temperature variations and show the spatial distribution of the primary thermal sources: Joule effect, free-carrier absorption, non-radiative recombinations and quantum-well capture. The spatial mapping of each source might allow to limit the impact of self-heating on the performance.**

***Index Terms*—VCSEL, Heat equation, Physics-based**

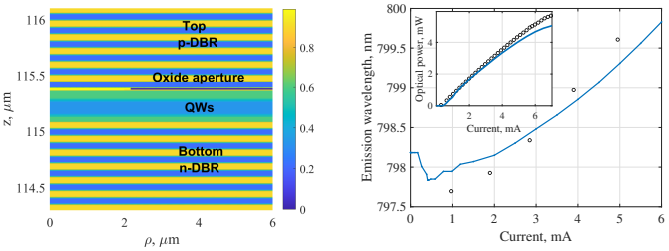

(a) Molar fraction in the cavity proximity.

(b) Wavelength red-shift vs bias current I. Inset: LI curve.

Fig. 1: (a) 2D molar fraction of the VCSEL under analysis and (b) validation of VENUS (solid curve) against experimental results (circles).

I. Introduction

Vertical-cavity surface-emitting lasers (VCSELs) serve as optical sources across a diverse set of applications, owing to their well-established advantages. High modulation bandwidth and circular beam profile pushed VCSELs adoption in short-reach, high-speed optical interconnects, particularly within data center environments [1]. Other applications ranging from gas sensing and atomic pumping to optical coherence tomography (OCT) for diagnostic imaging offer further lines of development for alternative applications. In these contexts, the output power of VCSELs is typically constrained by the limited size of their active region. Over the past decade, the need of a single-mode, narrow linewidth and large power coming from LiDARs (Light Detection And Ranging) technologies is pushing for novel design of VCSELs [2]. An instance is represented by multijunction VCSELs, that adopt tunnel junctions to cascade more active stages and enhance internal quantum efficiency and output power.

A common challenge for VCSELs regards self-heating, especially in continuous wave regime. Its primary evidence is the reduction of output power at the so called rollover current, related to the thermally induced gain peak shift, stronger leakage current and non-radiative recombination processes. Additionally, the thermally induced variation of the refractive index across the device shifts the emission wavelength towards red ($0.06 - 0.1$ nm K^{-1}) and increases the spatial confinement of the modes (thermal lensing), possibly hindering beam quality and modal purity. A proper heat management should rely on a thermal-aware design of VCSELs, as their capillary diffusion in different markets requires a well rounded understanding of every aspect of their operation to develop high-performance devices.

II. Results and Outlooks

To date, no experimental technique – whether destructive or non-destructive – possesses the capability of resolving the spatial distribution of self-heating within VCSELs. Experimentally, the sole accessible observable related to the temperature variation is the emission wavelength red-shift. This spectral measurement provides just an indirect glimpse, reflecting the averaged thermally induced modulation of the refractive index across the device.

Our in-house VCSEL static solver VENUS is capable of extracting and reproducing such experimental evidence for axisymmetric structures [3]. An example is reported in Fig. 1, where a standard industry-level oxide-confined ($\rho_{ox} = 2\,\mu$m) *pin* AlGaAs VCSEL with GaAs quantum wells (QWs) emitting at 795 nm (see refractive index profile in Fig. 1a) is simulated. In Fig. 1b, the agreement with experimental emission wavelength and output power (LI) as a function

TABLE I: Thermal conductivity values adopted in VENUS for different sections of the investigated VCSEL [5].

VCSEL region	κ ($\mathrm{Wm^{-1}K^{-1}}$)
Substrate	46
DBRs, active region, mesa (transv.)	15
DBRs, active region, mesa (long.)	12
Passivation	0.5

of current ensures that VENUS is estimating properly self-heating, adopting $dn/dT = 2.35 \cdot 10^{-4}$ K^{-1}.

All the solver details are not reported here, beside the static heat equation solved adopting the mortar element method [4] to compute the spatially-distributed temperature T variation from the heat sink [5], accounted imposing a homogeneous Dirichlet condition at the substrate:

$$\nabla \cdot (\kappa \nabla T) = -\underbrace{\left(\frac{J_n^2}{\sigma_n} + \frac{J_p^2}{\sigma_p}\right)}_{\text{Joule}} - \underbrace{\frac{dS_z(z)}{dz} \cdot P_{st} \cdot |\varepsilon(\rho)|^2}_{\text{FCA}} - \underbrace{qR_{nr}^{3D}(E_{fn} - E_{fp})}_{\text{NR recomb.}} - \underbrace{\left(qC_{cap}^{3D}(E_{fn} - E_{fp}) - R_{st}^{2D}\hbar\omega\right)}_{\text{capt./esc.}} \quad (1)$$

Here, κ denotes the non-linear thermal conductivity, whose values are reported in Table I. On the right hand side of (1), the expression for every thermal source is discussed afterwards. Each term is spatially dependent and comes from electrical (drift-diffusion, DD) and optical (electromagnetic) solvers.

In this way, VENUS locates the contribution from each thermal source in every point of the VCSEL mesh. In Fig. 2, we report their shape at a bias current of 5 mA. In Fig. 2a, the maximum temperature variations are reported as functions of current $\Delta T(I)$. The vertical line denotes 5 mA, and the inset shows the corresponding temperature longitudinal profile in the central section of the device.

The microscopic Ohm's law describes the Joule effect. It contains the squared current densities $J_{n,p}$ divided by the electrical conductivities $\sigma_{n,p}$. This explains the parabolic trend of $\Delta T_{Joule}(I)$, in blue in Fig. 2a. From Fig. 2c, the peak values arise at the oxide edge, where current crowding effect is relevant. The fringes stem from the DBRs heterointerfaces.

The free-carrier absorption (FCA) term contains the longitudinal derivative of the Poynting vector $S_z(z)$ – capturing the layer-by-layer absorption and the optical standing wave (SW) pattern, the output optical power P_{st} (explaining the linear $\Delta T_{FCA}(I)$, in red in Fig. 2a) and the emitted mode radial field shape $\varepsilon(\rho)$. In Fig. 2d, the fringes reflect the SW pattern, while the strong peak at the output facet comes from the highly absorptive GaAs contact layer.

The non-radiative (NR) recombination processes heating is modeled by multiplying Auger and SRH rates R_{nr}^{3D} by the elementary charge q and the quasi-Fermi level difference $E_{fn} - E_{fp}$. From Fig. 2a, their impact on the overall heating is very limited, and spatially located in the active region (Fig. 2e).

QW carrier capture is treated similarly to NR recombination. The capture rate C_{cap}^{3D} is responsible of filling QW states, acting as a quantum-correction to the bulk DD [3]. Most

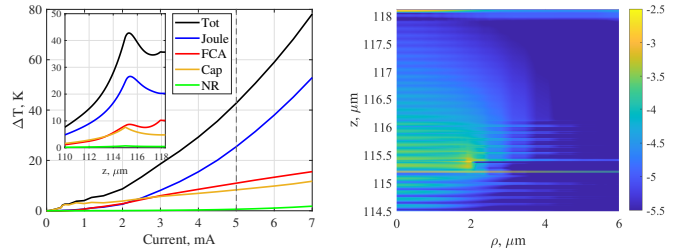

(a) ΔT vs I. Inset: $\Delta T(z)$ at 5 mA. (b) All sources

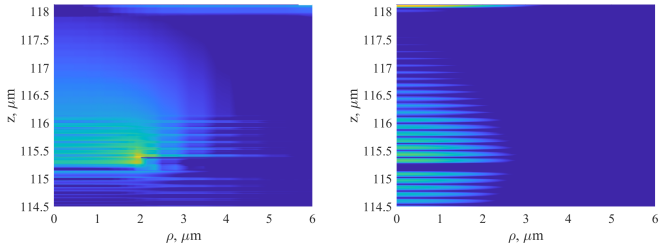

(c) Joule (d) FCA

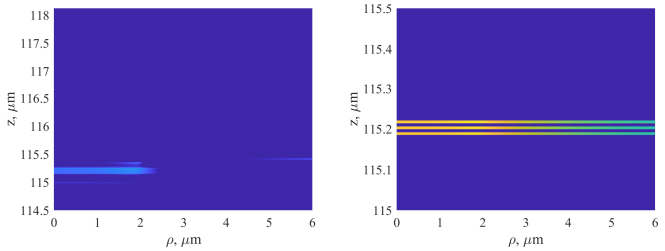

(e) Recombinations (f) Capture

Fig. 2: (a) Temperature variation ΔT vs current I. (b–f) Thermal sources (log. scale) extracted at 5 mA, from the n-DBR pairs next to the cavity up to the output facet (on top). The 2D maps share the same color scale.

captured carriers contribute to the stimulated emission at energy $\hbar\omega$, that is treated as a 2D recombination (R_{st}^{2D}). The net difference between these two terms models the capture heating, localized in the QW nodes (Fig. 2f). Its impact on the overall $\Delta T(I)$ in Fig. 2a, in yellow, quickly increases up to threshold ($I_{th} = 0.5$ mA). After I_{th}, QW populations should remain clamped, as they are balanced with the stimulated emission. Nevertheless, temperature-induced cavity losses demand higher QW carrier densities.

The strength of our thermal model is the possibility of describing each heating source separately. The evaluation of each spatial and current-dependent signature unlocks thermal-aware novel design for high temperature operations.

References

[1] N. N. Ledentsov, *et al.*, "High speed vcsel technology and applications," *J. Lightwave Technol.*, vol. 40, no. 6, pp. 1749–1763, 2022.

[2] I. Kim, *et al.*, "Nanophotonics for light detection and ranging technology," *Nature Nanotechnol.*, vol. 16, no. 5, pp. 508–524, 2021.

[3] A. Tibaldi, *et al.* "VENUS: a Vertical-cavity surface-emitting laser Electro-opto-thermal NUmerical Simulator," *IEEE J. Select. Topics Quantum Electron.*, vol. 25, no. 6, p. 1500212, Nov./Dec. 2019.

[4] A. Tibaldi, *et al.* "Skew incidence plane-wave scattering from 2-D dielectric periodic structures: analysis by the mortar-element method," *IEEE Trans. Microwave Theory Tech.*, vol. 63, no. 1, pp. 11–19, 2015.

[5] P. Debernardi, *et al.* "Probing thermal effects in VCSELs by experiment-driven multiphysics modeling," *IEEE J. Select. Topics Quantum Electron.*, vol. 25, no. 6, p. 1700914, Nov./Dec. 2019.